npj | quantum materials

Article

Published in partnership with Nanjing University

https://doi.org/10.1038/s41535-024-00677-9

Collapse of metallicity and high-T_c superconductivity in the high-pressure phase of $FeSe_{0.89}S_{0.11}$

Pascal Reiss [1,2] ✉, Alix McCollam[3], Zachary Zajicek [1], Amir A. Haghighirad [1,4] & Amalia I. Coldea [1] ✉

We investigate the high-pressure phase of the iron-based superconductor $FeSe_{0.89}S_{0.11}$ using transport and tunnel diode oscillator studies using diamond anvil cells. We construct detailed pressure-temperature phase diagrams that indicate that the superconducting critical temperature is strongly enhanced by more than a factor of four towards 40 K above 4 GPa. The resistivity data reveal signatures of a fan-like structure of non-Fermi liquid behaviour which could indicate the existence of a putative quantum critical point buried underneath the superconducting dome around 4.3 GPa. With further increasing the pressure, the zero-field electrical resistivity develops a non-metallic temperature dependence and the superconducting transition broadens significantly. Eventually, the system fails to reach a fully zero-resistance state, and the finite resistance at low temperatures becomes strongly current-dependent. Our results suggest that the high-pressure, high-T_c phase of iron chalcogenides is very fragile and sensitive to uniaxial effects of the pressure medium, cell design and sample thickness. This high-pressure region could be understood assuming a real-space phase separation caused by nearly concomitant electronic and structural instabilities.

In the quest of seeking higher and higher superconducting transition temperatures, the application of large hydrostatic pressures is an important tool. While the highest transition temperatures close to room temperatures were observed in conventional hydride superconductors under enormous pressures in the hundreds of gigapascal (GPa) range[1–3], much lower pressures in the tens of GPa range are sufficient to boost superconductivity in unconventional superconductors, most notably in the copper-based[4], the iron-based[5], and in the recently discovered nickel-based systems[6–8].

The family of the iron-chalcogenide FeSe has emerged as an enormously versatile system in which superconductivity can be tuned not only by hydrostatic pressure, but also by uniaxial strain, isovalent and charge doping, surface dosing, and chemical intercalation[9–17]. The richness of this system partially stems from its instability towards an electronic nematic phase at ambient conditions and its proximity to a magnetic phase which is stabilized under high pressures[11]. Remarkably, it is possible to disentangle the electronic nematic and magnetic phases through a careful combination of iso-electronic doping of $FeSe_{1-x}S_x$ with hydrostatic pressures[18], which allows one to study the contributions of their corresponding order parameter fluctuations to the superconducting pairing independently.

In particular, applied pressure studies of $FeSe_{0.89}S_{0.11}$ have provided unique access to an isolated nematic quantum critical point[19,20]. Towards higher pressures, multiple studies identified a strongly enhanced superconducting phase with the transition temperature T_c approaching values of $\approx$ 35 K[18]. However, the nature of this high-pressure phase and of the underlying electronic structure remains unclear, and previous studies produced partially contradictory results. In particular, a resistivity study reported enhanced superconductivity up to 8 GPa, and the emergence of a seemingly competing spin-density magnetic phase in the pressure range 2–4 GPa[18]. In contrast, a subsequent *ac* susceptibility study did not find signatures of any magnetic order but observed a complete loss of the superconducting shielding at 4 GPa[21]. Another recent transport and nuclear magnetic resonance (NMR) study detected weak signatures for magnetism above 3 GPa, and a gradual suppression of superconductivity beyond 4 GPa[22]. In $Cu_xFe_{1-x}Se$ only magnetism was suppressed under pressure but superconductivity remained strong[23], whereas in thin flakes of FeSe, an unusual suppression of the magnetic and superconducting phases under pressure with decreasing flake thickness was observed[24]. Similarly, the sample thickness and the choice of pressure medium were found to strongly

[1]Clarendon Laboratory, Department of Physics, University of Oxford, Oxford, UK. [2]Max Planck Institute for Solid State Research, Stuttgart, Germany. [3]High Field Magnet Laboratory (HFML-EMFL), Radboud University, Nijmegen, The Netherlands. [4]Institute for Quantum Materials and Technologies, Karlsruhe Institute of Technology, Karlsruhe, Germany. ✉e-mail: p.reiss@fkf.mpg.de; amalia.coldea@physics.ox.ac.uk

affect the boundaries of the superconducting phase in bulk FeSe above 5 GPa, likely due to additional uniaxial stress along the *c* direction[25].

In order to assess the nature of this enigmatic high-pressure phase in detail, we investigate $FeSe_{0.89}S_{0.11}$ via transport and tunnel diode oscillator (TDO) studies using opposing Diamond Anvil Cells (DACs), and different liquid pressure media up to ≈ 7 GPa. We find that the superconducting transition temperature T_c shows a minimum of 6 K around ≈ 1 GPa, before it increases towards 40 K above ≈ 4 GPa. Above 4 GPa, we observe significant changes in the sample properties. The room temperature normal state resistivity displays a sudden increase with pressure, whereas the low-temperature resistivity develops a marked fan of non-Fermi liquid behaviour. Further increasing the pressure, the resistivity develops non-metallic behaviour. Simultaneously, the superconducting transition broadens significantly until it becomes incomplete and fails to induce a zero-resistance state even at the lowest temperatures, together with an unusually small critical current density. This development is similar to FeSe, where non-metallic resistivity and a loss of superconductivity were observed under pressure above 10 GPa which were associated to a structural transition from tetragonal towards an orthorhombic or possibly hexagonal phase[11,26,27]. Our experimental findings in $FeSe_{0.89}S_{0.11}$ are consistent with a pressure-induced crossover from a metallic-like to a insulating-like behaviour which leads to a phase coexistence between superconducting/metallic and non-superconducting/semi-metallic domains. Within this picture, the observation of a quantum critical fan as a typical signature of a second-order electronic instability is unusual and it is potentially interrupted by the assumed structural instability.

Results

Superconducting phase

Previous studies have established that at ambient pressure $FeSe_{0.89}S_{0.11}$ becomes superconducting below a sharp transition temperature $T_c \approx 10.4$ K inside a nematic electronic phase below $T_s \approx 60$ K[14,19,20,22,28,29]. Upon application of hydrostatic pressure, the nematic transition temperature is quickly suppressed and a nematic quantum critical point is revealed around $p_c \approx 0.6$ GPa as determined at low temperatures (corresponding to approximately 0.8 GPa at the room temperature pressure, see the Methods section). Quantum oscillations have revealed the presence of a Lifshitz-like transition across the border of the nematic phase while the effective masses of the quasiparticles do not display divergent behaviour[19,29].

Figure 1a–d show the temperature dependence of the zero-field resistivity and TDO resonant frequency for different single crystals of $FeSe_{0.89}S_{0.11}$, using either Glycerol or a 4:1 mixture of Methanol:Ethanol as pressure media, up to pressures of ≈ 7 GPa. At the lowest pressure accessible with the Diamond Anvil Cell, the TDO data for 0.6(1) GPa shows a weak anomaly around 25 K, best visible as a dip in the temperature derivative shown in Fig. 1d. We associate this anomaly with the nematic phase transition, in good agreement with previous reports using piston cylinder cells[19]. Moreover, Fig. 1a–d reveal clear signatures of superconducting phase transitions as either a sharp drop in the resistance, or a surge in the TDO resonant frequency. Interestingly, above 4.2 GPa the superconducting transitions in the transport samples broaden significantly, and beyond 5 GPa, the transitions become incomplete as the sharp drop in the resistance does not lead to a zero-resistance state anymore, as shown in Fig. 1a. Therefore, in order to quantify the broadening effects and the loss of a fully superconducting phase, we will follow the evolution of four different anomalies in resistivity corresponding to the onset (T_c^{on}), sharpest drop (T_c^{p}), offset (T_c^{off}) and true zero resistance (T_c^{0}) temperatures, as indicated in Fig. 1e–f and the Methods section.

Figure 2 summarizes the evolution of the different superconducting and non-superconducting temperatures in a detailed pressure-temperature phase diagram for all single crystals of $FeSe_{0.89}S_{0.11}$ studied here and in previous reports[18,19,21,22,28]. At the lowest pressures, the superconducting transition temperatures T_c drop from ≈ 10 K at ambient pressure towards a minimum ≈ 6 K at a pressure of ≈ 1 GPa, independent of the pressure technique or medium employed. In the intermediate pressure regime between 1 GPa < $p \lesssim 4$ GPa, superconductivity is strongly enhanced and all critical temperatures continue to follow each other closely, reaching values close to 35 K at 4.0 GPa. However, in this regime, we find that T_c depends strongly on the pressure environment. As shown in Fig. 2(b), studies performed using opposing anvil cells and Glycerol, as in this report and in ref. 21, show excellent agreement in the value of T_c. In contrast, studies carried out using piston cylinder cells (PCC), such as sample P[19] and ref. 28, or cubic anvil cells using Glycerol[18], reported transition temperatures up to 10 K

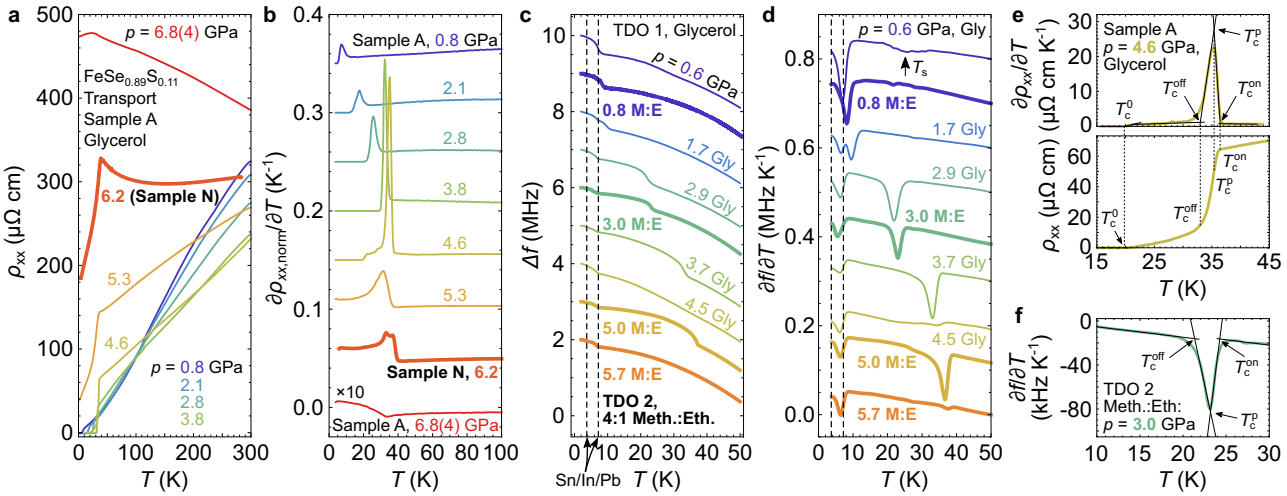

Fig. 1 | Evolution of the zero-field properties of $FeSe_{0.89}S_{0.11}$. **a** The temperature and pressure dependencies of the zero-field resistivities of samples A (thin lines) and sample N (thick line). The pressure transmitting medium for both samples is Glycerol. **b** First derivative of the low-temperature regime of panel (**a**) focusing on the superconducting transitions. Here, the resistivities are normalized against their values at $T = 100$ K and their derivatives shifted vertically for clarity. **c** Low-temperature evolution of the resonant frequency of a TDO circuit comparing the effects of either Glycerol as pressure transmitting medium (TDO1, 'Gly', thin lines), or a 4:1 mixture of Methanol:Ethanol (TDO2, 'M:E', thick lines). **d** First derivative of the TDO resonant frequency. T_s indicates the position of the nematic transition visible at lowest pressures. Vertical dashed lines in panels (**c**) and (**d**) indicate the pressure-independent superconducting transitions of In, Sn and Pb, which originate from the solder joints outside the pressure cell. **e**, **f** Definition of the superconducting critical temperatures indicated by arrows. The onset and offset temperatures, T_c^{on} and T_c^{off}, are defined where the derivative of the resistivity or the TDO resonant frequency recovers their high- and low-temperature values, respectively. The peak in the derivative defines T_c^{p}, and T_c^{0} is the temperature with truly zero resistance. At high pressures $p \gtrsim 4$ GPa, an additional low-temperature tail in resistivity leads to $T_c^{0} \ll T_c^{off}$.

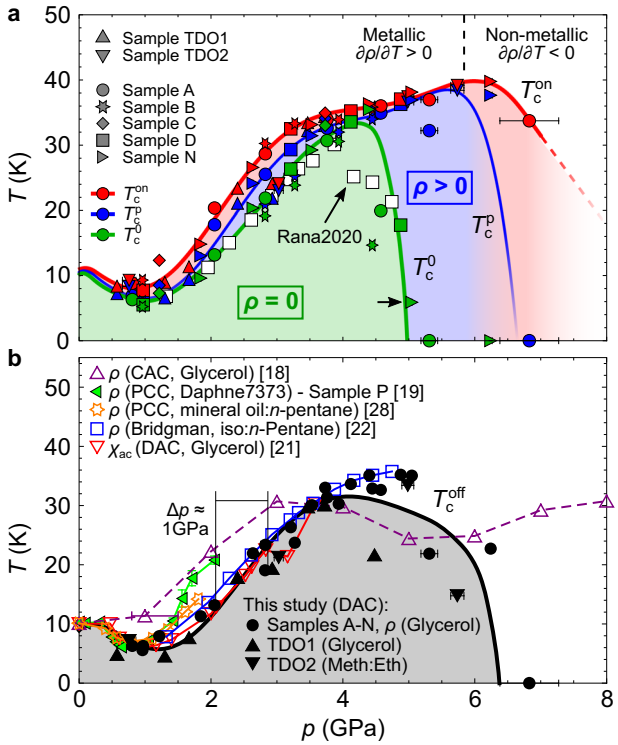

Fig. 2 | Pressure dependence of the different superconducting transition temperatures T_c. **a** The pressure dependencies of the onset temperature T_c^{on}, the temperature of the steepest change of the resistance or of the TDO signal T_c^{p}, and the zero-resistance temperature T_c^{0}. These transition temperatures start deviating from each other beyond ≈ 4 GPa. Points on the $T = 0$ line indicate that the associated transition temperature could not be observed. The open (white) symbols correspond to T_c^{0} from a previous report for $FeSe_{0.91}S_{0.09}$ in ref. 22. A strong current dependence is observed for the data point marked by an arrow (T_c^{0} of sample N at $p = 5.0$ GPa), as discussed in the main text. Thick solid lines are guide-to-the-eyes and the dashed line is a linear extrapolation. **b** Comparison of the offset superconducting transition temperatures T_c^{off} using different high-pressure methods, as reported here and previously. CAC = Cubic Anvil Cell, DAC = opposing Diamond Anvil Cell, PCC = Piston Cylinder Cell, Meth:Eth = 4:1 mixture of Methanol:Ethanol, ρ = transport study, χ_{ac} = AC susceptibility study[18,19,21,22,28]. Horizontal error bars indicate the pressure difference measured before cooldown and after warming up, but at least 0.1 GPa. Error bars associated with data from references are defined there.

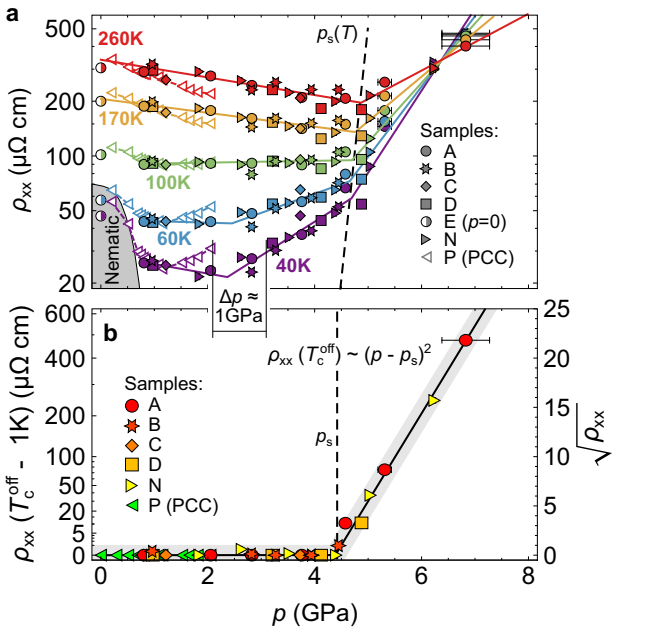

Fig. 3 | Correlation between resistivity increase and loss of superconductivity. **a** Absolute resistivity as a function of pressure at selected fixed temperatures. The horizontal bar indicates a pressure offset of $\Delta p \approx 1$ GPa between the data measured on sample P using a piston cylinder cell (open triangles) and the other samples using Diamond Anvil Cells (filled symbols). **b** Residual resistivity just below T_c^{off}. Solid lines are a guides to the eye. The dashed lines indicate the relevant pressure scale where kinks in the data appear. Horizontal error bars indicate the pressure difference measured before cooldown and after warming up, but at least 0.1 GPa.

higher, or equivalently shift the high-pressure, high-T_c phase to lower pressures by $\Delta p \approx 1$ GPa. Since the latter pressure techniques ensure a significantly higher hydrostatic environment than opposing anvil cells, the observed disparity between the studies suggests that superconductivity in this pressure regime sensitively depends on the strength of non-hydrostatic (uniaxial) pressure components.

In the high-pressure regime above ≈ 4 GPa, the critical temperatures display divergent trends. Figure 2 shows that the onset temperature T_c^{on} keeps increasing for all samples studied and reaches a maximum of 39.2 K around ≈ 6 GPa, remarkably similar to the maximum superconducting temperature of 38.3 K detected in FeSe at 6.3 GPa[13], and in the more heavily doped $FeSe_{0.83}S_{0.17}$ in the absence of the SDW phase[18]. In contrast, the zero-resistance critical temperature T_c^{0} and the temperature T_c^{p}, marking the sharpest drop in the resistivity or the surge in the TDO resonant frequency, respectively, become strongly sample dependent. On average, T_c^{0} drops quickly and vanishes around 5 GPa, consistent with a previous report[22], whereas T_c^{p} disappears around 6 GPa. Neither signature could be observed in any sample above 5 GPa and 6.5 GPa, respectively, as indicated in Fig. 2a. Such distinct pressure dependencies of the critical temperatures T_c^{0}, T_c^{p} and T_c^{on} suggest that the loss of superconductivity does not imply a closure of the gap, but rather an inhomogeneous and/or filamentary nature of superconductivity. This finding will be corroborated by the critical current studies that indicate a strongly reduced superconducting volume fraction, as discussed in Section ID. Moreover, the alteration of the superconducting phase is consistent with a previous *ac* susceptibility study which identified a weakened diamagnetic shielding in the same pressure regime[21].

Normal state resistivity

Mirroring the evolution of the superconducting transition temperatures with pressure, the normal behaviour of the resistivity is also very sensitive to the applied pressure in different regimes. To better quantify the electronic changes across various pressure ranges, Fig. 3a shows the isothermal evolution of the resistivity for all samples studied here. Initially, and at room temperature, the resistivity shows a continuous reduction for pressures $p \lesssim 5$ GPa which appears consistent with an increasing electronic bandwidth as the orbital overlaps increase. In contrast, the low-temperature resistivity shows a more nuanced pressure dependence. At the lowest pressures, below 1 GPa, a marked drop of the low-temperature resistivity is observed as the nematic phase is suppressed. This trend can be explained by a growing Fermi surface and a reduced quasiparticle mass, based on our previous high-pressure transport and quantum oscillation studies up to 2.2 GPa[19]. Additionally, scattering off nematic and/or spin fluctuations as well as nematic domain boundaries within the nematic phase may contribute to the low-pressure, low-temperature resistivity, but all effects get suppressed with increasing pressure[30–32]. Upon further increasing the pressure, the low-temperature resistivity shows an upturn around ≈ 1.2 GPa (sample P) or ≈ 2.2 GPa (samples A-N). The corresponding pressure difference $\Delta p \approx 1$ GPa between the resistivities of sample P (measured inside a piston cylinder cell) and samples A-N (opposing anvil cell) is consistent with the pressure difference of their superconducting transition temperatures, as discussed above. Interestingly, for an intermediate temperature ≈ 100 K, the resistivity appears essentially pressure independent between 1 GPa and 4 GPa, which corresponds to the visible crossing point of the resistivity curves in Fig. 1a, similar to previous reports[19,22]. Such a crossing could

correspond to an electronic crossover from incoherent to coherent transport predicted for a Hund's metal, a change in scattering or electronic correlations tuned by pressure[33] or temperature-dependent effects induced by the shift of the chemical potential at high temperatures above 100 K[34].

Towards highest pressures, the evolution of the resistivity changes significantly at all temperatures. Figure 3a shows an upturn in the resistivity at a weakly temperature dependent pressure scale $p_s(T)$ which varies between $p_s(40\,\mathrm{K}) \approx 4.6$ GPa and $p_s(260\,\mathrm{K}) \approx 4.9$ GPa. Since p_s can be identified up to room temperature, we propose it as a signature of a potential pressure-induced structural transition. Furthermore, Fig. 3(b) shows the residual resistivity just below the offset temperature T_c^{off} which we found to be zero for pressures below $p_s(T_c^{off})$. However, for higher pressures, the development of a finite resistivity gradually appears, which illustrates the collapse of the zero-resistivity superconducting state at $p_s(T_c^{off}) \approx 4.4$ GPa. Towards higher pressures, this residual resistivity keeps growing roughly as $(p - p_s)^2$, consistent with the emergence of the low-temperature resistive tail below the main superconducting transition, visible in Fig. 1a. Eventually, the resistivity displays only an anomaly resembling a partial superconducting transition beyond ≈ 5 GPa, as discussed above. This unusual loss of superconductivity is similar to previous studies of FeSe, where it was associated with a structural transition into orthorhombic or possibly hexagonal phases[11,26,27]. Furthermore, the loss of superconductivity in FeSe was also induced by the Cu-substitution which could lead to the formation of an electronically inhomogeneous phase, having superconducting islands[17]. Therefore, the evolution of the normal and superconducting behaviour of $FeSe_{0.89}S_{0.11}$ at p_s could be driven by a potential structural transition, like in FeSe, or the development of an electronic phase separation.

Importantly, the weakly temperature-dependent pressure $p_s(T)$, at which there are substantial changes in the resistive and superconducting properties of $FeSe_{0.89}S_{0.11}$, is similar to the hydrostatic limit of the employed pressure medium Glycerol at ≈ 5 GPa[35]. In order to test the influence of the pressure medium, we have performed a comparative study using the TDO technique with Glycerol and with a 4:1 mixture of Methanol:Ethanol, which ensures hydrostatic conditions up to 10 GPa[35,36]. Figure 1c,d show the evolution of the resonant frequencies and their first derivatives, respectively, for both pressure media as a function of pressure and temperature. Since an estimation of the sample resistivity from the TDO frequency depends on precise knowledge of the experimental setup (sample and coil dimensions and any parasitic capacitance unavoidable in a pressure cell), we focus on the evolution of the superconducting transition only. Figure 1c,d reveal that superconductivity is significantly weakened for Glycerol from 4.5 GPa onwards, in excellent agreement with the transport samples using the same pressure environment. In contrast, for the much more hydrostatic mixture of Methanol:Ethanol, the suppression of bulk superconductivity occurs around 5.7 GPa. While this pressure is significantly higher than in the case of Glycerol as pressure transmitting medium, it is far below the hydrostatic limit of Methanol:Ethanol. Therefore, we infer that the loss of superconductivity and the increase in resistivity are not directly induced by the hydrostatic limits of the pressure transmitting media employed, but they appear to be intrinsic to the high-pressure electronic phase of $FeSe_{0.89}S_{0.11}$, even though the exact pressure is clearly influenced by the medium.

Beyond the clear changes in the resistive and superconducting properties as well as their mutual correlation as a function of pressure, our multiple studies do not reveal signatures of any additional phase transitions. We could not detect any thermodynamic transitions either, even though the TDO should in principle be capable of detecting such transitions, like in UTe_2[37]. For comparison, in the case of FeSe the resistivity displays kink-like signatures at the onset of a SDW phase above ≈ 0.8 GPa[11,25,28,38], whereas $FeSe_{0.88}S_{0.12}$ shows weak anomalies in resistivity in the range ≈ 5–7 GPa[18]. Furthermore, superconductivity survives in the high-pressure phase of $FeSe_{1-x}S_x$ when using a cubic anvil cell and no insulating behaviour occurs up to 8 GPa[11,18] which clearly differs from our observations. In contrast, the loss of superconductivity of $FeSe_{1-x}S_x$ and the absence of any long-range magnetic order was suggested using the *ac* susceptibility and a similar pressure technique to ours[21]. Moreover, high-pressure NMR studies could not reveal enhanced magnetic fluctuations up to 4 GPa, but indicated the possibility of short-range antiferromagnetic (AFM) order[31]. These seemingly contradictory results may point at a strong sensitivity of FeSe-based materials to uniaxial pressure arising from the thermal contraction of opposing anvil cells, as employed here[39,40] and in ref. 21, combined with the additional effect induced by the sample thickness[24,25].

Non-Fermi liquid behaviour

Despite the absence of a signature of any long-range phase transition in the temperature dependence of the resistivity and TDO resonant frequency, we observe strong changes in the normal state properties at low temperatures which indicate that our samples are in the proximity to a pressure-induced electronic instability. Figure 4 summarizes the presence of a clear fan of non-Fermi liquid behaviour in the normal state resistivity, which is often regarded as a hallmark of putative quantum critical behaviour[41]. The resistivity in the vicinity of p_s displays a power-law form $\rho(T) = \rho_0 + aT^k$ with $k \approx 0.75$ for multiple samples, ranging from the onset temperature of superconductivity up to ≈ 130 K, as shown on Fig. 4b. This exponent differs clearly from the Fermi liquid predictions with $k = 2$, which was observed only at lower pressures and temperatures close to the nematic quantum phase transition[19,20,42].

Figure 4b shows the pressure and temperature dependence of the exponent k which reveals a fan-like structure above the superconducting dome (for sample B) which is truncated from ≈ 5 GPa onwards due to the presence of the non-metallic behaviour (see Methods and the Supplementary Note for a discussion regarding the validity of the resistivity exponent in the high-pressure region). Inside the power-law fan $k \approx 0.75$ which is consistent with the temperature dependence shown in Fig. 4a. On the other hand, outside of the fan at lower pressures $k \approx 1.5$ consistent with previous reports[19,42]. By linearly extrapolating the low- and high-pressure fan boundaries to zero temperature, the fan collapses at $p_Q = 4.3(2)$ GPa, which is close to p_s. The presence of a fan-like dependence of the resistivity exponent is typically regarded as a strong indicator for the presence of a putative quantum critical point (QCP) buried underneath the superconducting dome. A potential candidate for such behaviour could be an antiferromagnetic QCP, suggested to exist in the $FeSe_{1-x}S_x$ under pressure, measured using a cubic anvil cell[11,18].

Figure 4c shows that the resistivity exponent k has similar values for all samples measured using DACs, but differs in the pressure dependence from sample P measured in the PCC. At the lowest pressures outside the nematic phase, we find $k \approx 1.5$ for the DAC, in excellent agreement with sample P measured inside the PCC, consistent with previous reports[19,42]. With increasing pressure, the exponent k is reduced continuously upon entering the quantum critical fan and reaches a minimum of $k = 0.75 \pm 0.1$ at $p_Q = 4.3(2)$ GPa. Evidently, there is a sizable pressure offset in the evolution of k in sample P by $\Delta p \approx 1$ GPa (estimated at 2 GPa in Fig. 4c), consistent with those in T_c and the absolute value of ρ measure in the PCC, shown in Figs. 2b and 3b.

Figure 4d inset provides an additional test of the location of the quantum critical fan close to p_Q, based on the extracted values for ρ_0 (obtained from fits to a power law with fixed $k = 0.75$, in Fig. 4a). For small pressures $p < p_Q$, ρ_0 appears negative which is nonphysical, in contrast to larger pressure $p > p_Q$ where ρ_0 is positive. This implies that at low pressures ($p < p_Q$) the resistivity must have a larger exponent than $k = 0.75$ at low temperatures. Indeed, Fermi liquid behaviour with $k = 2$ was detected previously in the vicinity of the nematic quantum phase transition[19,20]. The resulting crossover Fermi temperature, T_{FL}, lies in a range of ≈ 10–20 K (as detailed in Methods) (see Fig. 4d), similar to our previous estimate close to the nematic quantum critical point where $T_{FL} = 11$ K was extracted for sample P[19].

Finally, we note that the extracted value of the resistivity exponent $k \approx 0.75 = 3/4$ is unusual and differs from typical values for ferromagnetic or antiferromagnetic quantum criticality, in either 2D or 3D, and for clean or

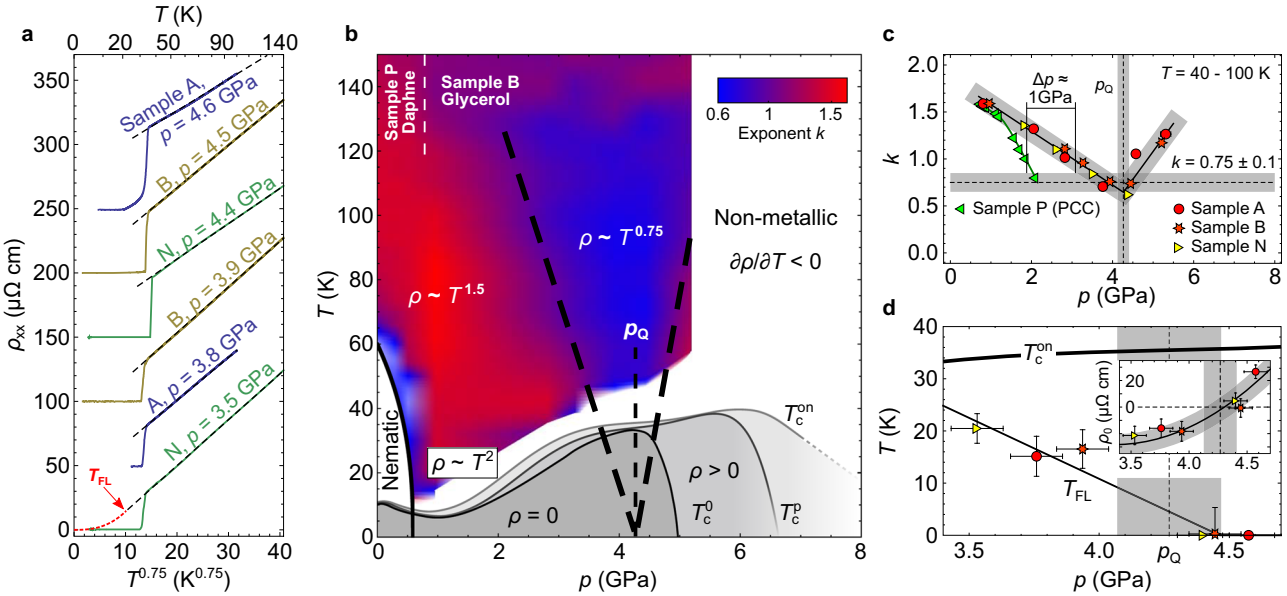

Fig. 4 | Non-Fermi liquid behaviour in pressurized $FeSe_{0.89}S_{0.11}$ above the superconducting dome. a Longitudinal resistivity $\rho_{xx}(T)$ of samples A, B and N plotted against $T^{0.75}$ for pressures close to the maximum of T_c^0. Straight dashed lines are linear fits and the red dotted line indicates assumed Fermi liquid behaviour at lowest temperatures. Curves are vertically offset for clarity. **b** Resistivity exponent k as obtained by the logarithmic derivative of $\partial\rho/\partial T$ of sample B as a function of temperature and pressure. A clear fan with $k \approx 0.75$ is observed above the superconducting dome reaching up to ≈ 130 K, whereas $k \approx 1.5$ outside the fan at low pressures. Black dashed lines indicate the boundaries of the fan and their intersection at a pressure p_Q at zero temperature. Only close to the suppression of the nematic phase and at the lowest temperatures, Fermi liquid behaviour with $k = 2$ was resolved in earlier studies[19,20]. **c** Resistivity exponent k obtained by fitting the experimental data using $\rho_{xx}(T) = \rho_0 + aT^k$ over the fixed temperature interval 40–100 K, outside the nematic phase. The horizontal dashed line indicates the best estimate for k at the minimum and its experimental uncertainty. The vertical dashed line indicates the extrapolated critical pressure p_Q as obtained from panel (b). The finite size horizontal bar indicates a pressure offset $\Delta p \approx 1$ GPa between the data obtained from sample P measured inside a PCC, and the other samples measured inside DACs. Vertical error bars indicate the 1σ confidence intervals. **d** The pressure dependence of the Fermi liquid temperature, T_{FL}, and the superconducting onset temperature T_c^{on}. The inset shows the residual resistivity ρ_0 obtained from fits using $k = 0.75$ which changes sign at p_Q. Vertical error bars indicate the standard deviation of T_{FL} and ρ_0 from varying $k \pm \delta k$ with $\delta k = 0.1$. Solid lines are guides-to-the-eye and the vertical dashed lines represents p_Q. Horizontal error bars indicate the pressure difference measured before cooldown and after warming up, but at least 0.1 GPa.

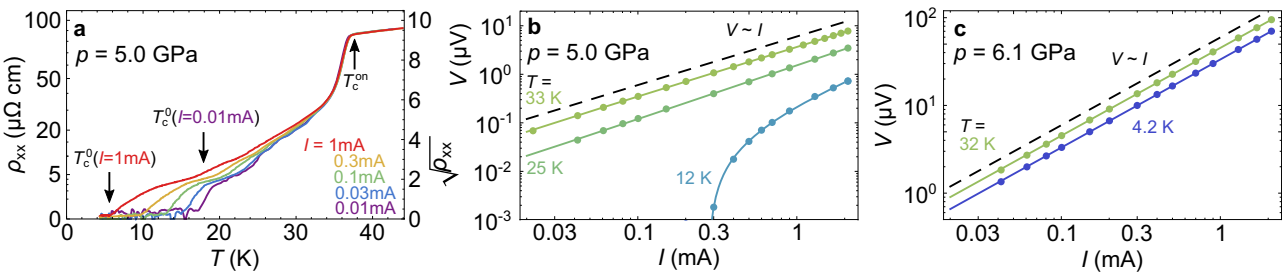

Fig. 5 | Critical current study in the high-pressure phase of $FeSe_{0.89}S_{0.11}$ for sample N. a The temperature dependence of zero-field resistivity during cooling as a function of applied current I under a pressure of $p \approx 5.0$ GPa. The position of T_c^0 (zero-resistivity temperature) depends strongly on the value of the applied current. **b**, **c** I–V-curves as a function of temperature for $p = 5.0$ GPa panel (**b**) and $p = 6.1$ GPa panel (**c**). The solid lines are guide-to-the-eyes. The dashed black line is a linear dependence $V \sim I$ indicating an ohmic resistance.

dirty systems[43,44]. Hence, we cannot infer the nature of the QCP from this value. However, theoretical predictions for quantum critical exponents in transport measurements actually relate to the temperature dependence of the scattering rate τ^{-1}, and not to the resistivity ρ. Since the resistivity $\rho \sim m^\star\tau^{-1}/n$ also depends on the charge carrier concentration n and the effective mass $m^\star$, an explicit temperature dependence of these quantities will alter the observed resistivity exponent k. Indeed, FeSe and related systems display a strong temperature dependence of the chemical potential[34] which manifests as a variation of the charge carrier density as a function of temperature. Additionally, inside the nematic phase, anisotropic scattering due to spin fluctuations may also become important[45,46]. Further magnetotransport studies will be required to assess changes in scattering in the high-pressure phase of $FeSe_{1-x}S_x$.

I–V characteristic

We now turn to the nature of the high-pressure ($p > p_Q$), low-temperature phase which displays a finite but incomplete superconducting phase. In order to separate normal metallic from partially superconducting resistances, we perform an I–V study to search for non-ohmic conduction and to determine the superconducting critical current density. Assuming an inhomogeneous superconducting phase with only filamentary superconducting paths, we would expect a strongly reduced critical current density j, when measured across the entire sample, which should be the smallest close to T_c. Figure 5a shows cooling curves on sample N at a pressure of 5.0 GPa under different applied currents across the broad superconducting transition. At this pressure, the sample shows a distinct superconducting onset, and eventually a zero resistance for all currents

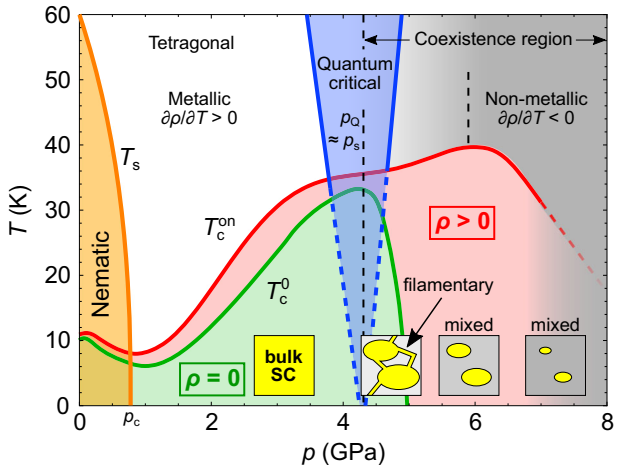

Fig. 6 | Proposed phase diagram covering the nematic, superconducting, tetragonal, quantum critical and coexistence regions. Real space sketches indicate how the superconducting volume fraction is lost.

studied (see also Fig. 2). However, in contrast to expectations, we find a strongly current-dependent sample resistivity only for temperatures below ≈ 25 K, whereas close to the onset temperature, T_c^{on}, the resistivity is essentially current independent, as shown in Fig. 5b. By increasing the pressure towards 6.2 GPa, shown in Fig. 5c, we observe ohmic resistance at all temperatures, despite a continuously well defined superconducting onset and sharp drop in the zero-field resistivity, (see Fig. 1a). This demonstrates that the high-pressure, low-temperature phase beyond $p_s > p_Q$ cannot be simply understood as filamentary superconductivity, but a more complex model is required, as discussed below.

Discussion

Our high-pressure study of the superconducting and normal state properties of $FeSe_{0.89}S_{0.11}$ reveals a complex pressure-temperature phase diagram, as summarized in Fig. 6. At very low pressures, the system displays a well-established nematic order (below T_s and p_c)[19,20], before it becomes superconducting below 10 K. Outside the nematic phase, T_c first reaches a minimum of 6 K at a pressure of 1 GPa, before it surges towards ≈ 40 K with increasing pressure. At high pressures beyond 4 GPa, the superconducting transition first becomes broader and eventually incomplete, whilst the onset temperature T_c^{on} keeps increasing until 6 GPa. At the same time, there are certain signatures in our transport data which suggest nearly concomitant electronic and structural instabilities. Firstly, we uncover clear signatures of non-Fermi liquid behaviour at $p_Q = 4.3(2)$ GPa which suggests the presence of an electronic quantum critical point. Secondly, reaching up to room temperature, the resistivity shows a marked upturn at $p_s(T) \approx 4.6$–4.9 GPa, and the system develops a non-metallic temperature dependence which cuts off the quantum critical fan emerging from p_Q (see also the Supplementary Note). Thirdly, the unusual low-temperature I–V dependence beyond p_s clearly suggests a loss of the superconducting volume fraction, consistent with a previous *ac* susceptibility study[21].

The signatures of the high-pressure phase could be explained considering a phase separation scenario, as sketched in Fig. 6. At low pressures, $p < p_s$, the superconducting phase has sharp superconducting transitions and reaches the zero-resistance state, as shown in Fig. 1a. Moreover, there is a large change in the TDO resonant frequency, as evident from Fig. 1c, and a sizable response in a previous *ac* susceptibility study[21]. Therefore, this low-pressure superconducting phase reflects the bulk nature of the superconducting state of the single crystals. In contrast, in the high-pressure phase, a finite resistance remains at lowest temperatures which displays clear non-ohmic behaviour only close to $p_s \gtrsim p_Q$, whereas the onset of the superconducting transition remains sharp and the finite resistance displays ohmic behaviour. This suggests that for temperatures just below T_c^{on}, only isolated superconducting islands develop within an emerging non-metallic matrix but they fail to connect to provide a fully superconducting current path. Thus, a drop in the resistance is observed when the islands become superconducting, and any finite resistance measured in this temperature regime arises solely from the normal state non-metallic matrix. In this case, the resistance would have ohmic behaviour and T_c^{on} should essentially be current independent, as observed in Fig. 5. Upon further lowering the temperature, the remaining normal state matrix gradually develops filamentary connections between the superconducting islands, which induce a strongly current-dependent phase and non-ohmic resistance, as observed in Fig. 5. With increasing pressure, the superconducting islands shrink and gradually disappear which makes a filamentary connection unlikely. This development is fully consistent with the remaining but shrinking sharp drop of the sample resistance at T_c^{on} even under a pressure of 6.2 GPa, the fully ohmic resistance observed at any temperatures, and the lack of a zero-resistance phase. By increasing the pressure even further, the islands are lost eventually, and the drop in resistance disappears, as shown in Fig. 1a.

The occurrence of a phase separation across p_s is consistent with a structural first-order transition. Yet, the observation of signatures associated with quantum criticality at $p_Q \lesssim p_s$ implies a second-order transition. The coexistence of such distinct transitions is highly unusual. Previous studies on $FeSe_{1-x}S_x$ crystals have reported both pressure-induced structural transitions at room temperature as well as electronic instabilities at low temperatures at very distinct pressures. For example, FeSe displays signatures of a low-temperature SDW phase in the pressure range ≈ 2–6 GPa which occurs together with a weak orthorhombic lattice distortion associated with the onset of the magnetic order. Yet, the system remains metallic in this pressure regime[11,27,47]. In contrast, a room temperature structural instability from tetragonal towards orthorhombic and hexagonal phases in FeSe could be induced only at much higher pressures above 10 GPa where non-metallic behaviour was observed[11,26,27]. Similarly for $FeSe_{0.88}S_{0.12}$, it was suggested that a SDW phase is stabilized in the pressure range ≈ 4–7 GPa from transport data anomalies, but no signatures of a non-metallic phase emerge at high pressures when using a cubic anvil cell[18]. A pressure-induced structural instability was detected for a similar compound at room temperatures beyond 9 GPa only[48]. Furthermore, this assumed phase separation is consistent with a proposed short-range AFM phase under pressure, as suggested recently by an NMR study[31].

One interesting aspect amongst the pressure studies of $FeSe_{1-x}S_x$ is that any discrepancies reported could be related to the different pressure media and pressure cell designs used in the experiments, and the varying sample thicknesses. In the case of structural studies, often Helium is used as pressure medium which ensures a much more hydrostatic environment as compared with Glycerol and the 4:1 Methanol:Ethanol mixture used here[27,48]. Indeed, our TDO study demonstrates that the choice of pressure medium has a measurable effect. While superconductivity is lost around 4 GPa close to the solidification pressure of Glycerol[35], it survives to a significantly higher pressures of ≈ 5 GPa using a 4:1 mixture of Methanol:Ethanol as pressure medium[35,36]. However, since the latter solidifies around 10 GPa only, this suggests that the structural and electronic instabilities are not directly triggered by the solidification of the pressure media during pressurisation at room temperature (i.e. the nominal hydrostatic limit). Instead, the pressure cell designs and their different thermal contractions could play a major role. By design, cubic anvil cells and piston cylinder cells are less prone to building up uniaxial pressure components due to their thermal contractions compared to the opposing anvil cell used here[39,40]. As a result, transport measurements using a cubic anvil cell display a persistent zero-resistivity state beyond 4 GPa even when Glycerol is used[11,18]. In contrast, studies performed with opposing anvil cell designs revealed a gradual loss of superconductivity around 4 GPa and show good agreement with our study[21,22]. The role of thermal contractions is further evidenced by our reported temperature dependence of $p_s(T)$, which drops from 4.9 GPa close to room temperature to 4.6 GPa around 40 K, as shown in Fig. 3a. This drop is consistent with a small (presumably uniaxial) pressure component building up during cooldown which originates from the thermally shrinking pressure cell. The

different degrees of hydrostaticitiy between varying pressure cell designs is further corroborated by the consistent pressure offsets of $\Delta p \approx 1$ GPa in the absolute resistivity ρ, the superconducting transition temperatures T_c and the resistivity exponent k when comparing results from piston cylinder (PCC) and cubic anvil cells (DAC) on one hand, and opposing anvil cells on the other hand.

Therefore, our detailed comparison of pressure media and cell designs suggests that the concomitant structural and electronic instabilities could arise from finite uniaxial pressure components unavoidable in an opposing anvil cell setup. This conclusion is further supported by previous studies which demonstrated that the sample thickness and the choice of pressure medium can have profound influence on the stability of the SDW phase in FeSe[24,49]. Therefore, it is conceivable that finite uniaxial pressures along the crystallographic c axis might trigger a structural transition at p_s. Indeed, many iron-based superconductors are very sensitive to uniaxial pressure components[50] and the electronic structure changes significantly with varying chalcogen height, h, above the conducting Fe plane ($h = z \cdot c$, *where z is the Se position above the Fe plane*)[51,52].

A consequence of the possible first-order structural transition at p_s and the concomitant second-order electronic transition of possibly magnetic origin around p_Q is the inherent domain formation. This would naturally lead to additional scattering of the charger-carriers, and to a growing resistivity, as observed. Interestingly, the resistivity trends observed under pressures can be compared with the evolution of the resistivity in the presence of strong impurity scattering in $Cu_xFe_{1-x}Se$[17,53]. The primary effect of the Cu-substitution is to disturb significantly the charge carrier transport in the Fe plane, and thus to lead to a significant enhancement of scattering. As a result, the resistivity shows similar enhancements both in temperature dependence and in absolute values, as compared with those in the high-pressure phase, and additionally there is a strong reduction of charge carrier mobilities[17,23]. On the other hand, the superconductivity is strongly reduced in FeSe with increasing Cu content and only weak superconducting islands remain[17]. Under applied pressure, the signatures associated with the long-range magnetic order of FeSe are also washed out in $Cu_xFe_{1-x}Se$, suggesting the sensitivity of the high-pressure electronic phases to disorder and pressure effects[23].

In summary, we have explored the high-pressure phase of the iron-based superconductor $FeSe_{0.89}S_{0.11}$. Our transport and TDO measurements revealed a strongly enhanced superconducting phase at high pressures, which gradually disappears beyond ≈ 4.5 GPa as the system becomes non-metallic. This trend suggests the development of a phase separation triggered by an uniaxial pressure component which could induce a structural transition. At low temperatures, we revealed a fan-like structure of non-Fermi liquid behaviour towering above the superconducting phase which points towards a putative quantum critical point buried below. Our results also reveal the occurrence of electronic phase separation due to the assumed structural (first-order) and accidentally concomitant electronic (second-order) phase transitions. This could explain the strongly reduced critical current density of the superconducting phase. The effects reported here emphasize the sensitivity of high-T_c superconductivity of iron-chalcogenides to the structural and electronic degrees of freedom induced by uniaxial and hydrostatic pressures. Clearly, future experimental structural studies, e.g. Raman spectroscopy or x-ray diffraction could provide essential insights into the structural dependence of $FeSe_{1-x}S_x$ systems on the pressure medium and pressure cell design employed.

Methods

Experimental details

Single crystals of $FeSe_{1-x}S_x$ with $x = 0.11$ sulphur substitution were grown using the $KCl/AlCl_3$ chemical vapour transport method as described elsewhere[54]. High-pressure measurements were carried out using an opposing Diamond Anvil Cell (DAC) with a design similar to refs. 39,40, using 800 μm bevelled culets. BeCu gaskets with an initial thickness between 400 and 450 μm were pre-indented to $\approx$ 80 μm, and were subsequently drilled to produce a pressure chamber with a diameter of 400 μm. A thin layer of Stycast 1266:Alumina mixture was applied as gasket insulation, and the gasket was drilled again with a diameter of 350 μm. A total of five single crystals, all roughly $150 \times 70 \times 30$ μm^3, in dimensions were subjected to high-pressure transport measurements inside the DAC using Glycerol as pressure medium, measured to a maximum pressure of approximately 7 GPa. Samples A and B were measured using a standard 4 contact configuration with the voltage contacts placed onto one of the longest sample edges to determine the longitudinal resistivity. For samples C and D, the voltage contacts were placed on opposing edges of the sample suitable for a Hall effect measurement. Sample N was measured using a 5 contact setup, allowing simultaneous longitudinal and Hall effect measurements. For comparison in the low-pressure limit, sample E was measured under ambient pressure only, whereas Sample P was measured inside a piston cylinder cell (PCC) using Daphne Oil 7373 as pressure transmitting medium, as previously reported in refs. 19,20 (called Sample A there). The maximum pressure for sample P was 2.05 GPa in accordance with the hydrostatic limit of Daphne Oil 7373. All transport measurements were carried out using the AC LockIn technique with a low frequency and a low excitation current $I_p = 1$ mA within the (ab) plane, unless stated otherwise. For the determination of the samples resistivities, the ambient pressure and room temperature sample dimensions were used, and a small pressure-induced contraction of the samples along the crystallographic c direction of $\Delta c/c \approx 1\%$ GPa^{-1} was neglected[48].

A further two single crystals were studied using the Tunnel Diode Oscillator (TDO) technique, using either Glycerol (TDO1) or a 4:1 mixture of Methanol:Ethanol (TDO2) as pressure media. The latter ensures hydrostatic conditions up to 10 GPa, well beyond the highest pressure reported here, whereas the former shows non-hydrostatic behaviour from 4–6 GPa onwards[35,36,39,40]. In the TDO studies, we identify pressure-independent signatures associated with the superconducting transition temperatures of Pb, Sn and In, which occur in the solder joints outside the pressure cell. When they become superconducting, the quality factor of the LC circuit changes which affects the resonant frequency f. For the DACs, we used the Ruby fluorescence technique at room temperature to determine the pressure inside the cell using multiple small Ruby chips. The reported pressures here correspond to the average before and after cooldown, and error bars indicate the difference which was usually below 0.1 GPa. For the piston cylinder cell used for sample P, the pressure was determined from the superconducting transition temperature of Sn at low temperatures. In order to compare the low-T pressure scale of sample P reported before[19,20] with the room temperature pressure scales of the other samples reported here, the pressures determined for sample P were shifted by +0.2 GPa for $p < 1$ GPa and +0.1 GPa for $p < 2$ GPa to account for the pressure losses of Daphne 7373 during cool-downs. All high-pressure measurements were carried out on compression. Pressures were changed at room temperature and the cells were allowed to relax until no change in pressure and the applied load could be resolved. Cooling rates were 0.5 K min^{-1} except for sample N where higher rates were used. The noise level in the TDO measurements is usually below 100 Hz. Any additional transitions can only be detected within this limit.

Superconducting transition temperatures

For a quantitative assessment of the evolution of superconductivity, we define four different superconducting transition temperatures, as exemplified in Fig. 1e,f. Firstly, by fitting the derivatives of the resistivity and the TDO resonant frequency, $\partial\rho/\partial T$ or $\partial f/\partial T$, respectively, the onset temperature T_c^{on} is extracted from the crossing of tangents fitted to the high-temperature normal state data and the leading edge of the superconducting transition. Secondly, the peak temperature T_c^p where the first derivatives show a maximum or minimum, respectively, is extracted from the crossing of tangents fitted to the leading and trailing edges of the transition. Thirdly, the offset temperature T_c^{off} is defined analogously to T_c^{on}, but using the trailing edge and the low-temperature data. Fourthly, we extract the true zero-resistance temperature T_c^0 when the signal falls below the noise level.

Extraction of resistivity exponents and T_F

To trace the pressure and temperature regimes where the exponent $k = 0.75$ provides a valid description of the resistivity, we extract k using a second derivative method as $k = 1 + \partial/\partial(\log T)(\partial\rho/\partial T)$. A key advantage of this method is that it is independent of the knowledge of ρ_0 which is often unreliable to extract from high-temperature data.

The estimation of the lower bound of the Fermi liquid crossover temperature, T_{FL}, is obtained by matching smoothly a physically limiting model for Fermi liquid behaviour $\rho_{FL}(T) = a_{FL}T^2$ (with the boundary case $\rho_{0,FL} \to 0$) with the experimentally extracted high-temperature power-law behaviour $\rho_n(T) = \rho_0 + a_nT^n$ (where mathematically we allow $\rho_0 < 0$). In this case, T_{FL} is defined through $\rho_{FL}(T_{FL}) = \rho_n(T_{FL})$ and $\partial\rho_{FL}/\partial T|_{T_{FL}} = \partial\rho_n(T)/\partial T|_{T_{FL}}$ which yields $T_{FL} = \left(\frac{2\rho_0}{a_n(n-2)}\right)^{1/n}$. This procedure yields a lower bound for T_{FL}, which indicates the lowest temperature below which a strictly Fermi liquid behaviour would give $\rho_0 = 0$, as shown in Fig. 4(a).

Data availability

For the purpose of Open Access, the author has applied a CC BY public copyright licence to any Author Accepted Manuscript version arising from this submission. In accordance with the EPSRC policy framework on research data, the data that support the findings of this study are available through the ORA (Oxford University Research Archive) at https://doi.org/10.5287/ora-6g0op82z9.

Received: 6 March 2023; Accepted: 13 August 2024;
Published online: 30 September 2024

References

1. Drozdov, A. P., Eremets, M. I., Troyan, I. A., Ksenofontov, V. & Shylin, S. I. Conventional superconductivity at 203 kelvin at high pressures in the sulfur hydride system. *Nature* **525**, 73–76 (2015).
2. Drozdov, A. P. et al. Superconductivity at 250 K in lanthanum hydride under high pressures. *Nature* **569**, 528–531 (2019).
3. Grockowiak, A. D. et al. Hot hydride superconductivity Above 550 K. *Front. Electron. Mater.* **2**, 837651 (2022).
4. Chu, C. W. et al. Superconductivity above 150 K in $HgBa_2Ca_2Cu_3O_{8+\delta}$ at high pressures. *Nature* **365**, 323–325 (1993).
5. Sun, L. et al. Re-emerging superconductivity at 48 kelvin in iron chalcogenides. *Nature* **483**, 67–69 (2012).
6. Sun, H. et al. Signatures of superconductivity near 80 K in a nickelate under high pressure. *Nature* **621**, 493–498 (2023).
7. Li, Q. et al. Signature of superconductivity in pressurized $La_4Ni_3O_{10}$. *Chin. Phys. Lett.* **41**, 017401 (2024).
8. Puphal, P. et al. Unconventional crystal structure of the high-pressure superconductor $La_3Ni_2O_7$. *arXiv*: 2312.07341 (2023).
9. Ge, J.-f. et al. Superconductivity above 100 K in single-layer FeSe films on doped $SrTiO_3$. *Nat. Mater.* **14**, 285–289 (2014).
10. Burrard-Lucas, M. et al. Enhancement of the superconducting transition temperature of FeSe by intercalation of a molecular spacer layer. *Nat. Mater.* **12**, 15–19 (2013).
11. Sun, J. P. et al. Dome-shaped magnetic order competing with high-temperature superconductivity at high pressures in FeSe. *Nat. Commun.* **7**, 12146 (2016).
12. Wen, C. H. P. et al. Anomalous correlation effects and unique phase diagram of electron-doped FeSe revealed by photoemission spectroscopy. *Nat. Commun.* **7**, 10840 (2016).
13. Sun, J. P. et al. High-T_c superconductivity in FeSe at high pressure: dominant hole carriers and enhanced spin fluctuations. *Phys. Rev. Lett.* **118**, 147004 (2017).
14. Reiss, P. et al. Suppression of electronic correlations by chemical pressure from FeSe to FeS. *Phys. Rev. B* **96**, 121103(R) (2017).
15. Farrar, L. S. et al. Suppression of superconductivity and enhanced critical field anisotropy in thin flakes of FeSe. *npj Quantum Mater.* **5**, 29 (2020).
16. Ghini, M. et al. Strain tuning of nematicity and superconductivity in single crystals of FeSe. *Phys. Rev. B* **103**, 205139 (2021).
17. Zajicek, Z. et al. Drastic effect of impurity scattering on the electronic and superconducting properties of Cu-doped FeSe. *Phys. Rev. B* **105**, 115130 (2022).
18. Matsuura, K. et al. Maximizing T_c by tuning nematicity and magnetism in $FeSe_{1-x}S_x$ superconductors. *Nat. Commun.* **8**, 1143 (2017).
19. Reiss, P. et al. Quenched nematic criticality and two superconducting domes in an iron-based superconductor. *Nat. Phys.* **16**, 89–94 (2020).
20. Reiss, P., Graf, D., Haghighirad, A. A., Vojta, T. & Coldea, A. I. Signatures of a quantum Griffiths phase close to an electronic nematic quantum phase transition. *Phys. Rev. Lett.* **127**, 246402 (2021).
21. Yip, K. Y. et al. Weakening of the diamagnetic shielding in $FeSe_{1-x}S_x$ at high pressures. *Phys. Rev. B* **96**, 020502 (2017).
22. Rana, K. et al. Impact of nematicity on the relationship between antiferromagnetic fluctuations and superconductivity in $FeSe_{0.91}S_{0.09}$ under pressure. *Phys. Rev. B* **101**, 180503 (2020).
23. Zajicek, Z., Singh, S. J. & Coldea, A. I. Robust superconductivity and fragile magnetism induced by the strong Cu impurity scattering in the high-pressure phase of FeSe. *Phys. Rev. Res.* **4**, 043123 (2022).
24. Xie, J. et al. Fragile pressure-induced magnetism in FeSe superconductors with a thickness reduction. *Nano Lett.* **21**, 9310–9317 (2021).
25. Miyoshi, K. et al. Disappearance and survival of superconductivity in FeSe under high pressure. *J. Phys. Soc. Jpn.* **90**, 073706 (2021).
26. Medvedev, S. et al. Electronic and magnetic phase diagram of β-$Fe_{1.01}Se$ with superconductivity at 36.7 K under pressure. *Nat. Mater.* **8**, 630–633 (2009).
27. Svitlyk, V. et al. Complex biphase nature of the superconducting dome of the FeSe phase diagram. *Phys. Rev. B* **96**, 014520 (2017).
28. Xiang, L. et al. Dome of magnetic order inside the nematic phase of sulfur-substituted FeSe under pressure. *Phys. Rev. B* **96**, 024511 (2017).
29. Coldea, A. I. et al. Evolution of the low-temperature Fermi surface of superconducting $FeSe_{1-x}S_x$ across a nematic phase transition. *npj Quantum Mater.* **4**, 2 (2019).
30. Wiecki, P. et al. Persistent correlation between superconductivity and antiferromagnetic fluctuations near a nematic quantum critical point in $FeSe_{1-x}S_x$. *Phys. Rev. B* **98**, 020507 (2018).
31. Kuwayama, T. et al. Pressure-induced reconstitution of Fermi surfaces and spin fluctuations in S-substituted FeSe. *Sci. Rep.* **11**, 17265 (2021).
32. Rana, K. et al. Interrelationships between nematicity, antiferromagnetic spin fluctuations, and superconductivity: Role of hotspots in $FeSe_{1-x}S_x$ revealed by high pressure ^{77}Se NMR study. *Phys. Rev. B* **107**, 134507 (2023).
33. Haule, K. & Kotliar, G. Coherence-incoherence crossover in the normal state of iron oxypnictides and importance of Hund's rule coupling. *N. J. Phys.* **11**, 025021 (2009).
34. Rhodes, L. C., Watson, M. D., Haghighirad, A. A., Eschrig, M. & Kim, T. K. Strongly enhanced temperature dependence of the chemical potential in FeSe. *Phys. Rev. B* **95**, 195111 (2017).
35. Tateiwa, N. & Haga, Y. Evaluations of pressure-transmitting media for cryogenic experiments with diamond anvil cell. *Rev. Sci. Instr.* **80**, 123901 (2009).
36. Jayaraman, A. Diamond anvil cell and high-pressure physical investigations. *Rev. Mod. Phys.* **55**, 65–108 (1983).
37. Lin, W.-C. et al. Tuning magnetic confinement of spin-triplet superconductivity. *npj Quantum Mater.* **5**, 68 (2020).
38. Terashima, T. et al. Pressure-induced antiferromagnetic transition and phase diagram in FeSe. *J. Phys. Soc. Jpn.* **84**, 063701 (2015).
39. Moulding, O., Osmond, I., Flicker, F., Muramatsu, T. & Friedemann, S. Absence of superconducting dome at the charge-density-wave quantum phase transition in 2*H*-$NbSe_2$. *Phys. Rev. Res.* **2**, 043392 (2020).

40. Moulding, O., Muramatsu, T., Sayers, C. J., Da Como, E. & Friedemann, S. Suppression of charge-density-wave order in $TiSe_2$ studied with high-pressure magnetoresistance. *Electron. Struct.* **4**, 035001 (2022).
41. Löhneysen, H. V., Rosch, A., Vojta, M. & Wölfle, P. Fermi-liquid instabilities at magnetic quantum phase transitions. *Rev. Mod. Phys.* **79**, 1015–1075 (2007).
42. Bristow, M. et al. Anomalous high-magnetic field electronic state of the nematic superconductors $FeSe_{1-x}S_x$. *Phys. Rev. Res.* **2**, 013309 (2020).
43. Rosch, A. Interplay of disorder and spin fluctuations in the resistivity near a quantum critical point. *Phys. Rev. Lett.* **82**, 4280–4283 (1999).
44. Brando, M., Belitz, D., Grosche, F. M. & Kirkpatrick, T. R. Metallic quantum ferromagnets. *Rev. Mod. Phys.* **88**, 025006 (2016).
45. Farrar, L. S. et al. Unconventional localization of electrons inside of a nematic electronic phase. *Proc. Natl Acad. Sci.* **119**, 2200405119 (2022).
46. Watson, M. D. et al. Dichotomy between the hole and electron behavior in multiband superconductor FeSe probed by ultrahigh magnetic fields. *Phys. Rev. Lett.* **115**, 027006 (2015).
47. Kothapalli, K. et al. Strong cooperative coupling of pressure-induced magnetic order and nematicity in FeSe. *Nat. Commun.* **7**, 12728 (2016).
48. Nikiforova, Y. A. et al. Crystal structure and phase transitions at high pressures in the superconductor $FeSe_{0.89}S_{0.11}$. *J. Alloy. Compd.* **860**, 158419 (2021).
49. Miyoshi, K. et al. Enhanced superconductivity on the tetragonal lattice in FeSe under hydrostatic pressure. *J. Phys. Soc. Jpn.* **83**, 013702 (2014).
50. Gati, E., Xiang, L., Bud'ko, S. L. & Canfield, P. C. Hydrostatic and uniaxial pressure tuning of iron-based superconductors: insights into superconductivity, magnetism, nematicity, and collapsed tetragonal transitions. *Ann. Phys.* **532**, 2000248 (2020).
51. Moon, C.-Y. & Choi, H. J. Chalcogen-height dependent magnetic interactions and magnetic order switching in $FeSe_xTe_{1-x}$. *Phys. Rev. Lett.* **104**, 057003 (2010).
52. Morfoot, A. B. et al. Resurgence of superconductivity and the role of dxy hole band in $FeSe_{1-x}Te_x$. *Commun. Phys.* **6**, 362 (2023).
53. Gong, C., Sun, S., Wang, S. & Lei, H. Normal and superconducting state properties of Cu-doped FeSe single crystals. *Phys. Rev. B* **103**, 174510 (2021).
54. Böhmer, A. E., Taufour, V., Straszheim, W. E., Wolf, T. & Canfield, P. C. Variation of transition temperatures and residual resistivity ratio in vapor-grown FeSe. *Phys. Rev. B* **94**, 024526 (2016).

Acknowledgements

We thank Sven Friedemann and Patricia Alireza for their valuable technical support setting up the high-pressure techniques in Oxford. We further acknowledge Matthew Watson for his previous measurement of sample E. This work was funded in part by the UKRI EPSRC (EP/I004475/1, EP/I017836/1). P.R. and A.A.H. acknowledge financial support of the Oxford Quantum Materials Platform Grant (EP/M020517/1). Part of this work was supported by HFML-RU and LNCMI-CNRS, members of the European Magnetic Field Laboratory (EMFL) and by EPSRC (UK) via its membership to the EMFL (grant no. EP/N01085X/1). We acknowledge financial support of Oxford University John Fell Fund. Z.Z. acknowledges financial support from the EPSRC studentship (EP/N509711/1 and EP/R513295/1). A.I.C. acknowledges an EPSRC Career Acceleration Fellowship (EP/I004475/1) and Oxford Centre for Applied Superconductivity.

Author contributions

A.I.C. and P.R. conceived the project. A.A.H. grew the single crystals. P.R. set up the high-pressure DAC measurements in Oxford. P.R., A.M., A.I.C and Z.Z. performed different measurements. P.R. analysed the data. P.R. and A.I.C. conceived the interpretation and wrote the manuscript with input from all authors.

Competing interests

The authors declare no competing interests.

Additional information

Supplementary information The online version contains supplementary material available at https://doi.org/10.1038/s41535-024-00677-9.

Correspondence and requests for materials should be addressed to Pascal Reiss or Amalia I. Coldea.